

The effects of different FRP/concrete bond–slip laws on the 3D nonlinear FE modeling of retrofitted RC beams – A sensitivity analysis

M. Lezgy-Nazargah*, M. Dezhangah and M. Sepehrinia

Department of Civil Engineering, Hakim Sabzevari University, Sabzevar 9617976487-397, Iran

(Received January 16, 2017, Revised September 16, 2017, Accepted November 11, 2017)

Abstract. The aim of this paper is to evaluate the accuracy and reliability of the available bond–slip laws which are being used for the numerical modeling of Fiber Reinforced Polymer (FRP)/concrete interfaces. For this purpose, a set of Reinforced Concrete (RC) beams retrofitted with external FRP were modeled using the 3D nonlinear Finite Element (FE) approach. All considered RC beams have been previously tested and the corresponding experimental data are available in the literature. The failure modes of these beams are concrete crushing, steel yielding and FRP debonding. Through comparison of the numerical and experimental results, the effectiveness of each FRP/concrete bond–slip model for the prediction of the structural behavior of externally retrofitted RC beams is assessed. The sensitivity of the numerical results against different modeling considerations of the concrete constitutive behavior and bond–slip laws has also been evaluated. The results show that the maximum allowable stress of FRP/concrete interface has an important role in the accurate prediction of the FRP debonding failure.

Keywords: debonding; FRP; bond–slip law; finite element; RC beam

1. Introduction

Due to useful mechanical properties (e.g., very high strength to density ratio, corrosion resistance, reduced maintenance costs and faster installation time compared to conventional materials), the FRP materials and in particular Carbon FRP (CFRP) materials are nowadays used extensively for repairing and rehabilitating of the reinforced concrete structures. They may be used for flexural strengthening of RC beams (Rahimi and Hutchinson 2001, Qeshta *et al.* 2015), shear strengthening of RC elements (Uriayer and Alam 2015, Panjehpour *et al.* 2014), and confinement of RC columns (Wang and Shao 2014, Zhou *et al.* 2014). Among these different applications, the use of CFRP as external reinforcement for flexural strengthening of concrete beams has received much attention from civil engineers. Tensile rupture of the CFRP laminates, debonding of the CFRP lamina from the substrate, and concrete crushing are the most important possible failure modes which have identified for externally strengthened beams through experimental tests (ACI 2002).

The accurate predictions of the failure mechanisms of the retrofitted RC beams using appropriate analytical and numerical methods are essential for design purposes. A literature study shows that many researchers have dedicated outstanding attention to this subject. Ziraba and Baluch (1995) studied the global behavior of externally retrofitted RC beams subjected to arbitrary load histories using a nonlinear FE code. In this reference, the concrete and FRP laminates are modeled using nine-node Lagrangian

elements. Three-node elements are employed for modeling the internal reinforcements. The interface between the concrete and internal and external reinforcements was also modeled using six-node interfacial elements. Using the commercial FE code ABAQUS, Arduini *et al.* (1997) analyzed eight FRP-strengthened RC beams under monotonic loading history. These researchers employed the smeared crack approach for the modeling of nonlinear behavior of concrete. They also assumed a perfect bond between the FRP and the concrete. Using a two-dimensional (2D) nonlinear FE code, Wong and Vecchio (2003) predicted the load–deflection behavior of FRP strengthened beams failing by laminate debonding. In this reference, the material nonlinearity of concrete is modeled using Modified Compression Field Theory. The interface between the FRP and concrete is also modeled using link and contact elements. Based on discrete segment analysis, Wang and Chen (2003) studied analytically the behavior of reinforced concrete T-beams retrofitted with CFRP plates. Coronado and Lopez (2006) studied the behavior of reinforced concrete beams strengthened with FRP laminates using the FE method. They investigated the effect of different modeling considerations of the concrete constitutive behavior on the numerical results. Chen *et al.* (2012) used an advanced FE model for predicting the shear behavior of RC beams shear-strengthened with FRP. They investigated the effects of different modeling assumptions for the interfaces between concrete and steel reinforcement, and between concrete and FRP. Biolzi *et al.* (2013) investigated delamination phenomena between a CFRP strip and a concrete substrate by means of single-lap shear specimens. Using a suitable FE model, Bencardino and Condello (2015) studied the effectiveness of some FRP/concrete bond–slip laws to model Steel Reinforced Grout-concrete

*Corresponding author, Associate Professor,
E-mail: m.lezgy@hsu.ac.ir; m.lezgy@yahoo.com

and/or Steel Reinforced Polymer-concrete interfaces. Using the commercial numerical analysis tool ABAQUS, Obaidat *et al.* (2010) developed an FE model for the analysis of beams retrofitted with CFRP. They used a cohesive model to represent the interfacial behavior between CFRP and concrete. Chen *et al.* (2012) studied the behavior of FRP/concrete interfaces between two adjacent cracks using FE method. The main objective of this reference (Chen *et al.* 2012) is to clarify the effects of damages of bondlines on the ultimate load of the bonded joint. Obaidat *et al.* (2013) presented a methodology for obtaining parameters describing bond action between FRP and concrete in RC structures strengthened in flexure. By employing a cohesive approach for modeling the interface between the external reinforcement and the substrate, Bocciarelli and Pisani (2015) proposed a modified force method for the nonlinear analysis of RC beams externally strengthened by FRP sheets.

Debonding of the FRP lamina from the concrete surface is one of the main issues which prevent the achievement of the full flexural capacity of the strengthened elements. Debonding always emanates from the formation and propagation of an interface crack in the adhesive layer between FRP and the substrate. In addition to debonding failure, even under service loads, significant slip occurs at the FRP/concrete interface which affects the structural responses of the strengthened beams (Abdel Baky *et al.* 2012, Mazzotti *et al.* 2008, Colombi *et al.* 2014). The review of the previous studies shows that the available approaches proposed for modeling the externally reinforced beams either assumes a perfect bond between the FRP and concrete or are not able to predict well the complete detachment of the FRP lamina from the substrate. In this work a detailed 3D nonlinear FE model using the ABAQUS code is developed for the accurate simulation of the structural response of retrofitted RC beams with different failure mechanisms. Special emphasis is placed on the modeling of the debonding failure mode. To this aim, the interface behavior between FRP and concrete substrate is modeled using different bond-slip laws (Obaidat *et al.* 2013, Monti *et al.* 2003, Lu *et al.* 2005, CNR-DT 2013, Neubauer and Rostasy 1999, Nakaba *et al.* 2001) available in the open literature. The effectiveness of these bond-slip laws for numerical simulations is evaluated through comparison with experimental results. Concrete damage plasticity (CDP) model is used for representing the nonlinear behavior of the concrete material. Elastic perfectly plastic behavior is employed for modeling the material nonlinearity of internal reinforcing steels whereas Hashin's failure criterion is used for determining the initiation of the failure in FRP sheets. The principal concrete material properties and interfacial parameters which affect the outcome of the numerical simulations are determined using the sensitivity analysis. The obtained results of this paper not only simplify the modeling procedure of the FRP detachment from the concrete substrate but also give a comprehensive view about different parameters of the CDP and CFRP/concrete bond-slip models.

2. Finite-element models

The numerical analysis was carried out by using the FE package ABAQUS/standard (Hibbitt *et al.* 2000). In this study, 8-node linear brick elements (C3D8R) were used for modeling the concrete. Reinforcing steels and FRP sheets were modeled using 2-node linear truss elements (T3D2) and 4-node doubly curved shell elements (S4R), respectively. The interaction between the concrete and FRP surfaces were defined using appropriate contact elements with cohesive behavior. A perfect bond is assumed at the interface between the steel reinforcements and concrete.

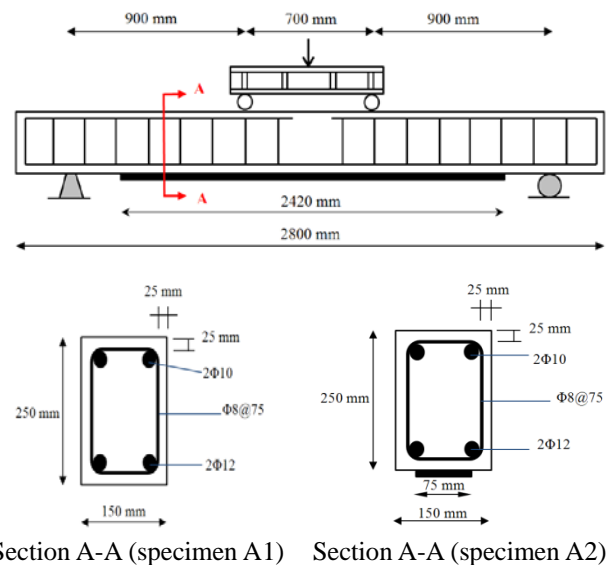
3. Experimental program

The FE models are verified against experimental data available in the open literature. A total of 4 RC beams with different mechanical and geometrical properties are selected for comparison with the numerical results.

The first experimental work considered in this study corresponds to a group of two RC beams tested under four-point bending: an un-strengthened (beam A1), and a beam simply strengthened with a unidirectional CFRP sheet (beam A2).

The used CFRP sheet has a thickness of 0.17 mm. Geometrical parameters and details of the external and internal reinforcements of these specimens are described in Fig. 1. The mechanical properties of the used concrete, steel and CFRP are also given in Table 1.

Another considered experimental work corresponds to two RC beams tested by Rahimi and Hutchinson (2001). These beams were tested under four-point bending. Beam B1 is used as a control specimen while beam B2 is strengthened with a CFRP sheet. Geometric properties and

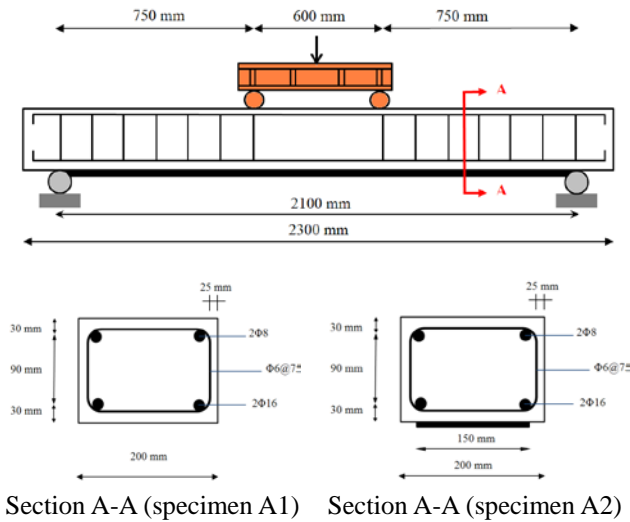


Section A-A (specimen A1) Section A-A (specimen A2)

Fig. 1 The detailed description of the geometry, loading conditions, internal and external reinforcements for RC beams series A (Qeshta *et al.* 2015)

Table 1 Material properties for RC beams Series A (Qeshta *et al.* 2015)

Mechanical property	Concrete	Steel rebar (Φ12)	Steel rebar (Φ10)	Steel stirrups	Epoxy	CFRP sheet
Modulus of elasticity (GPa)	39	210	210	210	4.5	230
Yield strength (MPa)	-	529	521	317	-	-
Compressive strength (MPa)	53	-	-	-	30	-
Tensile strength (MPa)	5.3	-	-	-	30	4900
Poisson's ratio	0.2	0.3	0.3	0.3	0.3	0.3



Section A-A (specimen A1) Section A-A (specimen A2)
 Fig. 2 Geometry and reinforcing details of the RC beams series B under four-point bending test (Rahimi and Hutchinson 2001)

internal and external reinforcements of these specimens are described in Fig. 2. Material properties are also given in Table 2. Note that the thickness of the used CFRP sheet is 4 mm.

4. Material constitutive behaviour

4.1 Concrete

A damaged plasticity model is used in this study for describing the stress-strain behavior of concrete in tension and compression. The yield function of the CDP model in terms of effective stresses takes the following form (Hibbitt *et al.* 2000, Lubliner *et al.* 1988, Lee and Fenves 1998)

$$F(\bar{\sigma}, \bar{\epsilon}^{pl}) = \frac{1}{1-\alpha} (\bar{q} - 3\alpha\bar{p} + \beta(\bar{\epsilon}^{pl})(\langle \bar{\sigma}_{max} \rangle - \gamma\langle \bar{\sigma}_{max} \rangle) - \bar{\sigma}_c(\bar{\epsilon}_c^{pl})) \quad (1)$$

In the above equation, \bar{p} is the hydrostatic pressure stress while \bar{q} denotes the Mises equivalent effective stress. $\bar{\epsilon}_t^{pl}$ and $\bar{\epsilon}_c^{pl}$ are equivalent plastic strains in tension and compression. Parameter α appeared in Eq. (1) can be calculated according to the following equation

$$\alpha = \frac{(f_{b0}/f_c) - 1}{2(f_{b0}/f_c) - 1} \quad (2)$$

where f_{b0} is the biaxial compressive strength of the concrete material and f_c is the uniaxial compressive strength. The function $\beta(\bar{\epsilon}^{pl})$ is given as

$$\beta(\bar{\epsilon}^{pl}) = \frac{\bar{\sigma}_c(\bar{\epsilon}_c^{pl})}{\bar{\sigma}_t(\bar{\epsilon}_t^{pl})} (1-\alpha) - (1+\alpha) \quad (3)$$

where $\bar{\sigma}_t$ and $\bar{\sigma}_c$ are the effective tensile and compressive cohesion stresses, respectively. Note that the Macauley bracket $\langle \cdot \rangle$ appeared in Eq. (1) is obtained as $\langle x \rangle = \frac{1}{2}(|x| + x)$. The parameter γ defines the shape of the yield surface. This parameter can be calculated as the below

$$\gamma = \frac{3(1-K)}{2K-1} \quad (4)$$

where K is the ratio of the tensile to the compressive meridian and defines the shape of the yield surface in the deviatoric plane.

For modeling the behavior of concrete under uni-axial compressive, the well-known stress-strain relationship of Hognestad (1951) is used. Concerning the stress-strain response of the concrete under uni-axial tension, a linear

Table 2 Material properties for RC beams Series B (Rahimi and Hutchinson 2001)

Mechanical property	Concrete	Steel	Epoxy	CFRP sheet
Modulus of elasticity (GPa)	25	210	7	127
Yield strength (MPa)	-	575	-	-
Compressive strength (MPa)	58.6	-	70	-
Tensile strength (MPa)	3	-	25	1532
Poisson's ratio	0.2	0.3	0.3	0.3

Table 3 Existing bond-slip models

Bond-slip model	K_0 (K/mm ³)	τ_{max} (N/mm ²)	G_f (N/mm)	β_w
Obidat <i>et al.</i> (2013)	$0.16 \frac{G_a}{t_a} + 0.47$	$1.46 G_a^{0.165} f_t^{1.033}$	$0.52 f_t^{0.26} G_a^{-0.23}$	-
Monti <i>et al.</i> (2003)	$\frac{E_a E_c}{2.5(t_a E_c + 50 E_a)}$	$1.8 \beta_w f_t$	$0.297 f_t \beta_w^2$	$\sqrt{\frac{1.5(2 - b_f/b_c)}{1 + b_f/100}}$
Lu <i>et al.</i> (2005)	76.92	$1.5 \beta_w f_t$	$0.308 \beta_w^2 \sqrt{f_t}$	$\sqrt{\frac{2.25 - b_f/b_c}{1.25 + b_f/b_c}}$
CNR-DT (2013)	$\frac{0.6}{\frac{t_a}{G_a} + \frac{25}{G_c}}$	$\frac{2G_f}{0.25}$	$\beta_w 0.077 \sqrt{f_t f_c}$	$\sqrt{\frac{2 - b_f/b_c}{1 + b_f/b_c}} \geq 1$
Neubauer and Rostasy (1999)	$8.91 f_t$	$1.8 \beta_w f_t$	$0.182 \beta_w^2 f_t$	$\sqrt{1.125 \frac{2 - b_f/b_c}{1 + b_f/400}}$
Nakaba <i>et al.</i> (2001)	$53.85 f_c^{0.19}$	$3.5 f_c^{0.19}$	$0.504 f_c^{0.19}$	-

elastic behavior is assumed until tensile strength (f_t) is reached. A linear softening behavior is also assumed for modeling the behavior of concrete after tensile crack initiation.

4.2 FRP model

In this study, the FRP behavior is assumed to be linear until failure. After failure, the FRP material losses all its load-carrying capacity. For predicting the occurrence of failures in FRP sheets, Hashin’s failure criterion (Hibbitt *et al.* 2000) is used. In contrast to other similar failure criteria (e.g., Maximum stress failure criterion, Maximum strain failure criterion, ...), Hashin’s failure criterion takes into account the interaction between stresses (Lezgy-Nazargah 2017).

4.3 Steel reinforcement

The constitutive behavior of steel in tension and compression is modeled using an elastic perfectly plastic model.

4.4 FRP/concrete interface model

Two different models are used for representing the interface between concrete and FRP. First, a perfect bond model is employed in order to have estimation about the structural behavior of the strengthened RC beams. Then, well-known bond-slip interface models proposed by different researchers (Obaidat *et al.* 2013, Monti *et al.* 2003, Lu *et al.* 2005, CNR-DT 2013, Neubauer and Rostasy 1999, Nakaba *et al.* 2001) were employed for describing the interaction behavior between the FRP and concrete. The considered interface models are based on traction-separation laws (cohesive behaviors). Traction-separation laws describe the interaction between two surfaces by defining a relative displacement at each contact point. A graphical representation of a traction–separation law is depicted in Fig. 3. In this figure, the vertical axis is effective traction while the horizontal axis denotes the effective

opening displacement. Both opening and sliding failure modes are considered for the interface behavior. It is worth to note that the opening mode is due to normal stresses while sliding failure mode depends on the shear stresses.

It can be observed from Fig. 3 that each traction-separation law is defined by three parameters: initial stiffness (K_0), normal (σ_{max}) or shear bond strength (τ_{max}), and fracture energy (G_f). The bond–slip laws considered in this study are summarized in Table 3. In Table 3, t_a denotes the resin thickness, b_f is FRP sheet width and b_c represents the concrete width. G_a and G_c are the shear modulus of resin and concrete, respectively. The modulus of elasticity of the resin and concrete are shown by E_a and E_c , respectively.

For determining the initiation of damage at the FRP/concrete interface, both Maximum stress and Quadratic

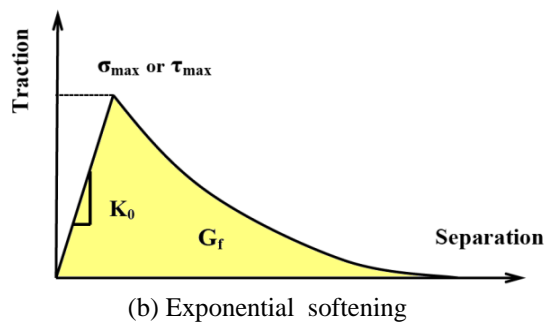
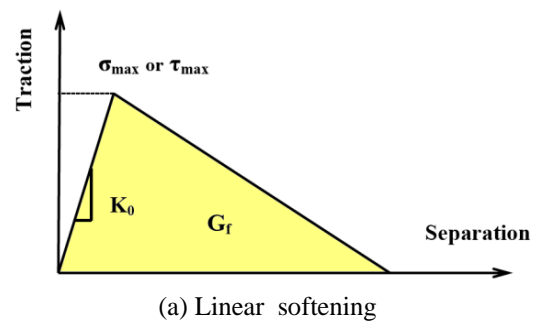


Fig. 3 FRP/concrete traction–separation relationship

stress criteria are used. According to the Maximum stress criterion (Hibbitt *et al.* 2000), the failure occurs when the maximum contact stress ratio defined in the following expression reaches the value one

$$\max \left\{ \frac{\langle \sigma_n \rangle}{\sigma_{n,\max}}, \frac{\tau_s}{\tau_{s,\max}}, \frac{\tau_t}{\tau_{t,\max}} \right\} = 1 \quad (5)$$

In the above equation, σ_n is the cohesive tensile, and τ_s and τ_t are the shear stresses at the interface. n represents the direction of the normal stress (opening mode) whereas s and t refer to the directions of the shear stress components at the interface. In Quadratic stress criterion (Hibbitt *et al.* 2000), the damage is assumed to initiate when the following quadratic traction function involving the contact stress ratios reached the value one

$$\left(\frac{\langle \sigma_n \rangle}{\sigma_{n,\max}} \right)^2 + \left(\frac{\tau_s}{\tau_{s,\max}} \right)^2 + \left(\frac{\tau_t}{\tau_{t,\max}} \right)^2 = 1 \quad (6)$$

In order to describe the damage evolution, both linear and exponential softening models expressed in terms of fracture energy (G_f) were used. For describing the dependency of the fracture energy to the opening and sliding failure modes, the Benzaggah–Kenane (BK) and power law (PL) fracture criteria were used. The PL criterion (Hibbitt *et al.* 2000) states that the failure under mixed-mode conditions is governed by a power law interaction of the energies required to cause failure in individual modes. This criterion can be represented by

$$\left(\frac{G_n}{G_f^n} \right)^\eta + \left(\frac{G_s}{G_f^s} \right)^\eta + \left(\frac{G_t}{G_f^t} \right)^\eta = 1 \quad (7)$$

In the above expression, the quantities G_n , G_s , and G_t denote the work done by the interfacial stresses and its conjugate separation in the normal, the first, and the second shear directions, respectively. η is a cohesive property parameter. G_f^n , G_f^s , and G_f^t represent the critical fracture energies required to cause failure in the normal, the first, and the second shear directions, respectively (in this study $G_f^n = G_f^s = G_f^t$). BK fracture criterion (Hibbitt *et al.* 2000) is given by

$$G_f^n + (G_f^s - G_f^n) \left(\frac{G_s + G_t}{G_n + G_s} \right)^\eta = G_f \quad (8)$$

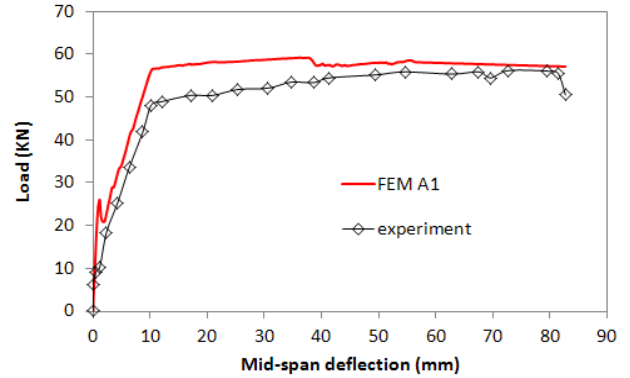
5. Results and discussions

5.1 Un-strengthened beam (A1 and B1)

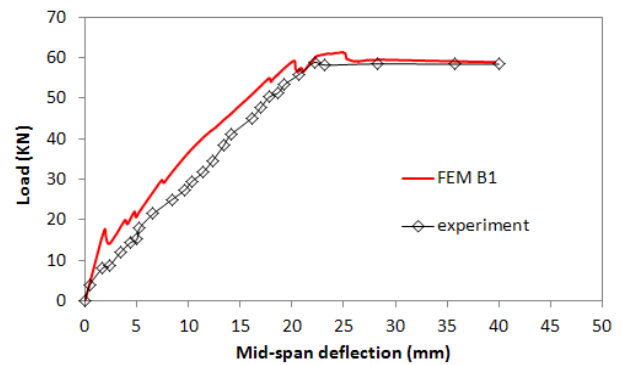
First, the failure behavior of un-strengthened RC beams A1 and B1 was investigated using the nonlinear FE analysis. The values used for the viscosity parameter (η), dilation angle (ψ), flow potential eccentricity (e), ratio of initial biaxial compressive yield stress to initial uniaxial

Table 4 The chosen values for the CDP parameters

ψ	e	f_{b0}/f_c	K	η
35°	0.5	1.16	0.667	0.0001



(a) Beam A1



(b) Beam B1

Fig. 4 Load-deflection response of un-strengthened RC beams

compressive yield stress (f_{b0}/f_c), and the ratio of the tensile to the compressive meridian (K) are given in Table 4. Fig. 4 presents the comparison between the FE and experimental results in terms of load–deflection response.

It is seen that the present FE results are in good agreement with experimental data. The error in the prediction of the failure load is less than 6%.

It is worthy to note that additional laboratory tests are required to find the proper values for the CDP parameters cited in Table 4. Unfortunately, there is no distinct theoretical approach for calculating the aforementioned parameters. However, the use of proper values for these parameters is essential for obtaining the proper and realistic results. The values used in Table 4 are selected after investigating of the sensitivity of the numerical solutions with respect to CDP parameters. These sensitivity analyses are explained in the subsequent sections.

5.1.1 Sensitivity to dilation angle

For stresses below the critical stress value (f_c), the Poisson’s ratio controls the volume changes of the concrete. After reaching the critical stress value, the concrete exhibits an increase in plastic volume under pressure (Chen 1982).

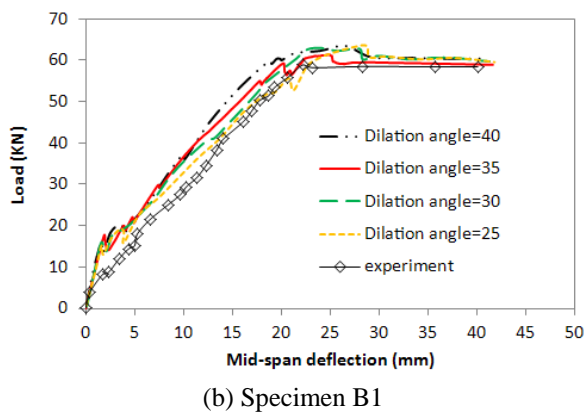
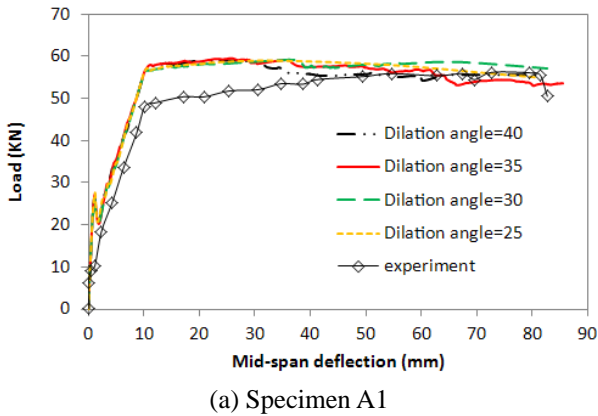


Fig. 5 Sensitivity to the angle of dilatancy

This behavior is taken into account in CDP model by defining the dilation angle parameter ψ . The recommended range of dilation angle for reinforced concrete in literature is between 20° to 40° (Lubliner *et al.* 1988). Based on this information, the angle of dilation was varied from 25° to 40° to see the sensitivity of the numerical results against it. The load-deflection curves of beam A1 and B1 are shown in Fig. 5. In these figures, the FE results are compared with experimental results. Depicted plots show that the numerical results are not varying dramatically as the dilation angle changes.

5.1.2 Sensitivity to f_{b0}/f_c

The sensitivity of the FE results against f_{b0}/f_c is investigated in this subsection. The parameter f_{b0}/f_c depends on the compressive strength and the confinement of concrete. Based on experimental tests, Kupfer *et al.* (1969) estimated this parameter as $f_{b0}/f_c = 1.16$. Numerical results for four different values of this parameter ($f_{b0}/f_c = 1, 1.16, 1.25$ and 2) are depicted in Fig. 6. It is seen that the results are not sensitive to the changes of this parameter.

In the load-deflection curves depicted in Figs. 4-6, three distinct stages can be observed. The first stage is related to the full elastic (uncracked) behavior of the RC beam. The load-deflection curve at this stage is almost a straight line which represents the full flexural rigidity of the RC beam. With the initiation of cracks in the critical sections of the RC beams, the second stage starts. At this stage, the tensile stresses in the tension zone of RC beam exceed the flexural strength of the concrete and consequently the flexural

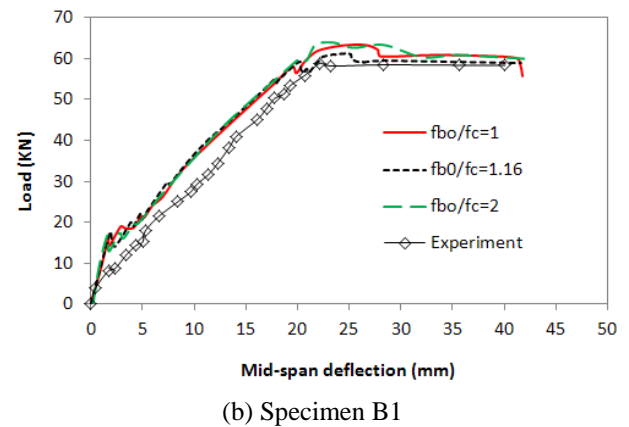
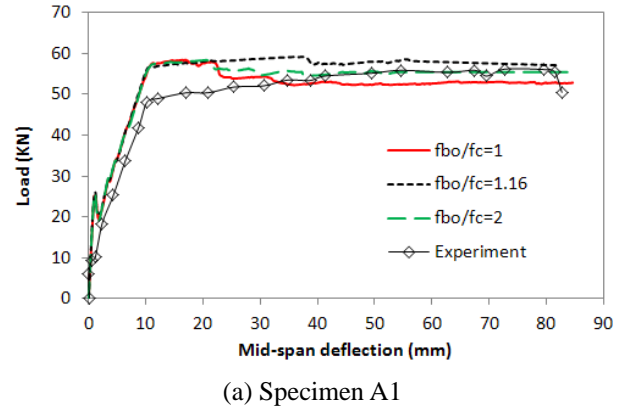


Fig. 6 Sensitivity to the ratio of initial biaxial compressive yield stress to initial uniaxial compressive yield stress

stiffness of the RC beam decreases. This can be observed by a sharp wave which appears after the initial stage of the simulated results. Finally, the third stage corresponds to the yielding of the steel reinforcements. At this stage, the load-deflection curve is almost smooth and the RC beam is assumed to have failed.

5.1.3 Sensitivity to eccentricity parameter

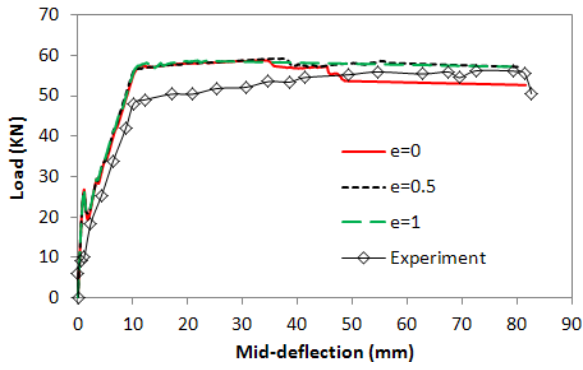
The flow potential eccentricity (e) controls the shape of the deviatoric section of the concrete yield surface. This parameter can be evaluated using the following formula (Lubliner *et al.* 1988)

$$e = \frac{1 + \varepsilon}{2 - \varepsilon} \quad \text{where} \quad \varepsilon = \frac{f_t}{f_{b0}} \frac{f_{b0}^2 - f_c^2}{f_c^2 - f_t^2} \quad (9)$$

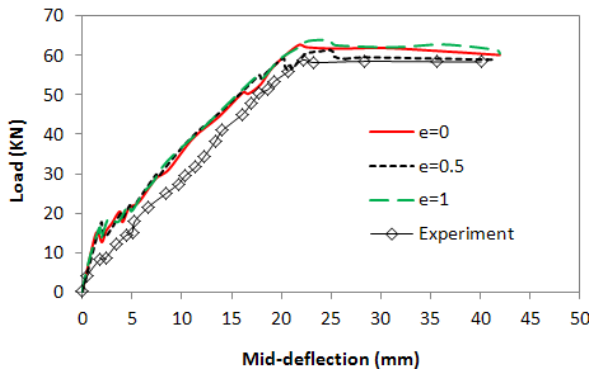
Due to the dependency of the f_{b0}/f_c to the experimental tests, Eq. (9) does not give a distinct value for this parameter. To this reason, the sensitivity of numerical results with respect to this parameter is studied here. The load-deflection of the RC beams A1 and B1 are shown in Fig. 7 for $e = 0$, $e = 0.5$ and $e = 1$. It can be observed that the numerical results are not significantly affected by this parameter.

5.1.4 Sensitivity to parameter K

Another parameter of the CDP model which is considered here is the ratio of the tensile to the compressive

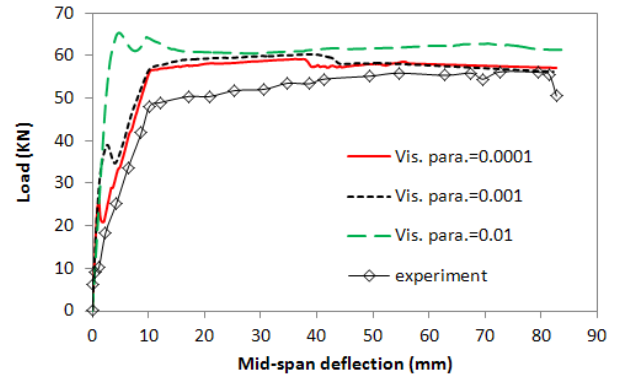


(a) Specimen A1

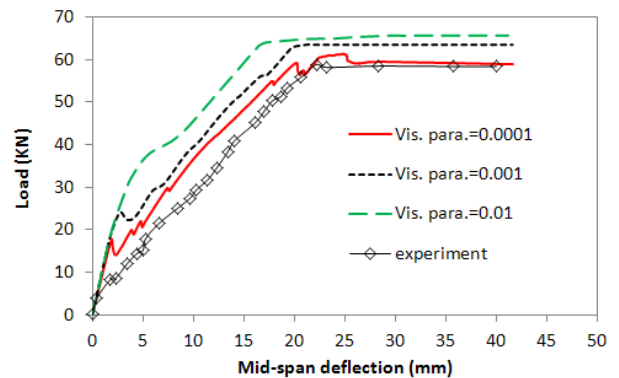


(b) Specimen B1

Fig. 7 Sensitivity to the eccentricity parameter

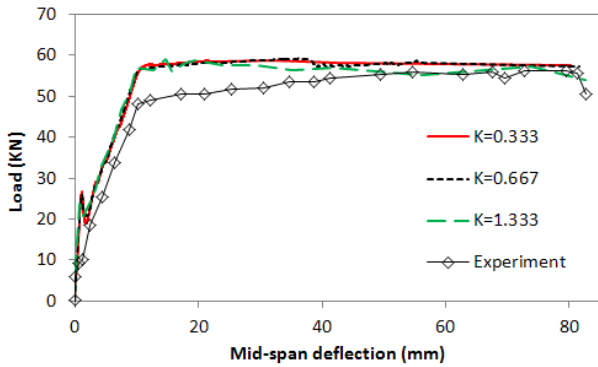


(a) Specimen A1

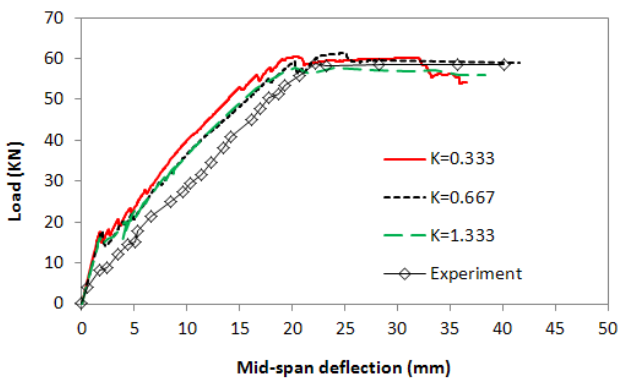


(b) Specimen B1

Fig. 9 Sensitivity to the viscosity parameter



(a) Specimen A1



(b) Specimen B1

Fig. 8 Sensitivity to the ratio of the tensile to the compressive meridian

meridian (K). This parameter defines the shape of the yield surface of concrete in the deviatoric plane. The load-deflection curves of un-strengthened RC beams A1 and B1 are depicted in Fig. 8 for $K = 0.333$, $K = 0.667$ and $K = 1.333$. Depicted graphs of Fig. 8 show that the FE results are not sensitive to the changes of this parameter.

5.1.6 Sensitivity to concrete tensile strength

Since different codes give various formulations for the calculation of the concrete tensile strength, the sensitivity of the numerical results against this parameter is investigated in Figs. 11(a) and (b). In these figures, the concrete tensile strength was changed from 0.5ft to 2ft. The numerical results show that the initial stiffness of RC beams increases slightly with increasing of the concrete tensile strength. However, this parameter does not have significant effect on the ultimate load capacity of the RC beams.

5.2 Strengthened beams (A2 and B2)

The failure behaviors of strengthened RC beams A2 and B2 are investigated in this section. The load-deflection curves of these beams predicted using seven different interface models are shown in Fig. 12. The experimental results are also given in these figures for evaluating the accuracy of the FE models. For the strengthened beams (A2 and B2), the values of the bond-slip parameters (K_0 , τ_{max} , G_f) were calculated according to the relationships of the considered cohesive models explained in Section 4.4. The

obtained input parameters are given in Table 5. They are employed for both opening and sliding fracture modes. For the calculation of the input parameters cited in Table 5, the initial thickness of the resin layer was put equal to $t_a =$

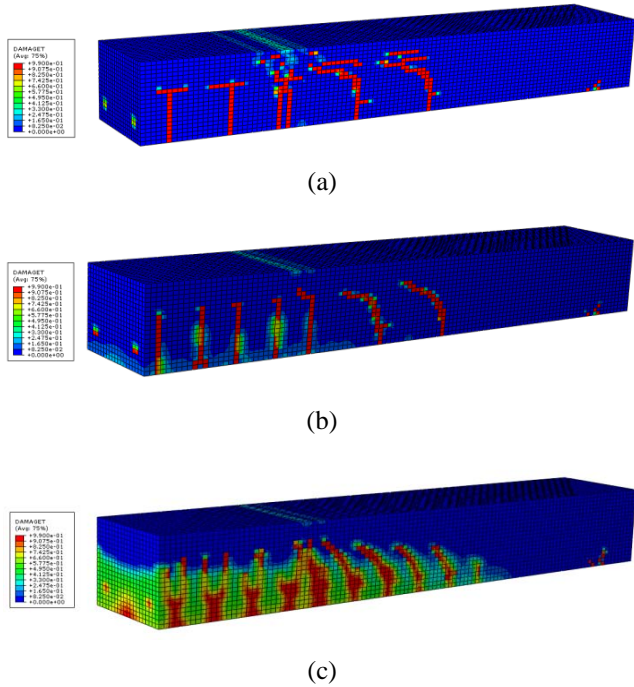


Fig. 10 The crack pattern of the RC beam B1 for different values of the concrete viscosity parameter: (a) $\eta = 0.0001$; (b) $\eta = 0.001$; (c) $\eta = 0.01$

1.0 mm. The Quadratic stress criterion is used for determining the initiation of damage at the CFRP/concrete interface. The power law fracture criterion with cohesive property coefficient $\eta = 1$ is also employed for describing the dependency of the fracture energy to the opening and sliding failure modes. To overcome the convergence difficulty commonly occurs in the modeling of debonding processes, the nonlinear problem is solved using the dynamic implicit method. The variable mass scaling technique was also used in all regions of the models to improve the computational efficiency. The solution time of each retrofitted beam model is approximately 72 hour using processor Intel(R) Core(TM) i7 (3.50 GHz).

It can be seen from Fig. 12 that different FE models predict the first part of the load-deflection curves very accurately. However, in the prediction of the second part of the load-deflection curves, they lead to different results. The perfect bond models overestimate the ultimate load capacity and the ductility of the retrofitted beams compared to experimental results. A perfect bond model also fails to capture the softening curves of the retrofitted RC beams. On the other hand, bond-slip interface models act better in the prediction of the softening branch of the retrofitted beams. After CFRP debonding failure, the bending capacity of the RC beams reduces to their bending capacity before strengthening. This phenomenon is captured well using the present bond-slip FE models. Fig. 12 shows that load-deflection curves predicted from the different bond-slip models are very similar. Moreover, the depicted graphs of Fig. 12 reveal this fact that the available bond-slip models predict the load capacity of the retrofitted RC beams lower than experimental ones. For example, the FE model based

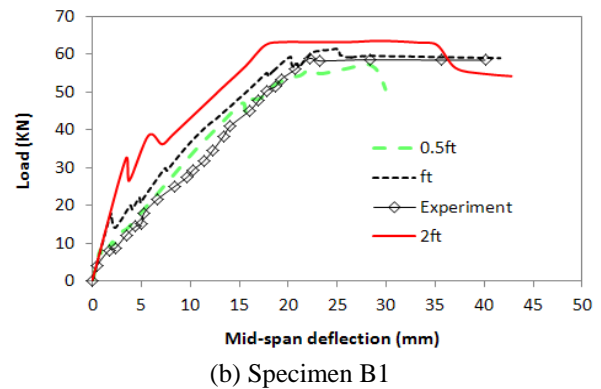
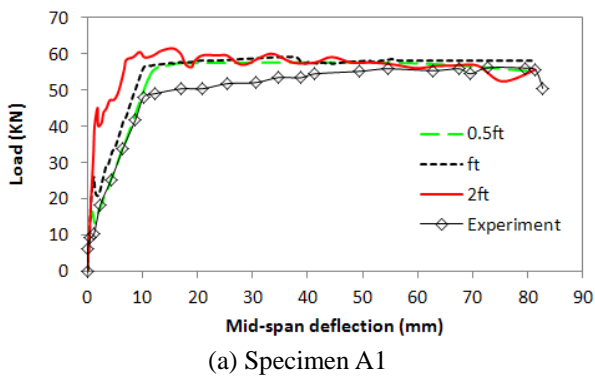


Fig. 11 Sensitivity to concrete tensile strength

Table 5 Input parameters of different bond-slip models)

Bond-slip model	Beam A2			Beam C2		
	K_0 (K/mm ³)	τ_{max} (N/mm ²)	G_f (N/mm)	K_0 (K/mm ³)	τ_{max} (N/mm ²)	G_f (N/mm)
Obidat <i>et al.</i> (2013)	746.92	8.95	0.71	900.77	5.35	0.55
Monti <i>et al.</i> (2003)	265.91	10.82	2.02	186.67	4.68	0.67
Lu <i>et al.</i> (2005)	76.92	7.95	0.71	76.92	3.90	0.40
CNR-DT (2013)	283.52	10.32	1.29	216.49	8.17	1.02
Neubauer and Rostasy (1999)	47.22	11.37	1.37	26.73	5.46	0.56
Nakaba <i>et al.</i> (2001)	114.50	7.44	1.07	116.70	7.59	1.09

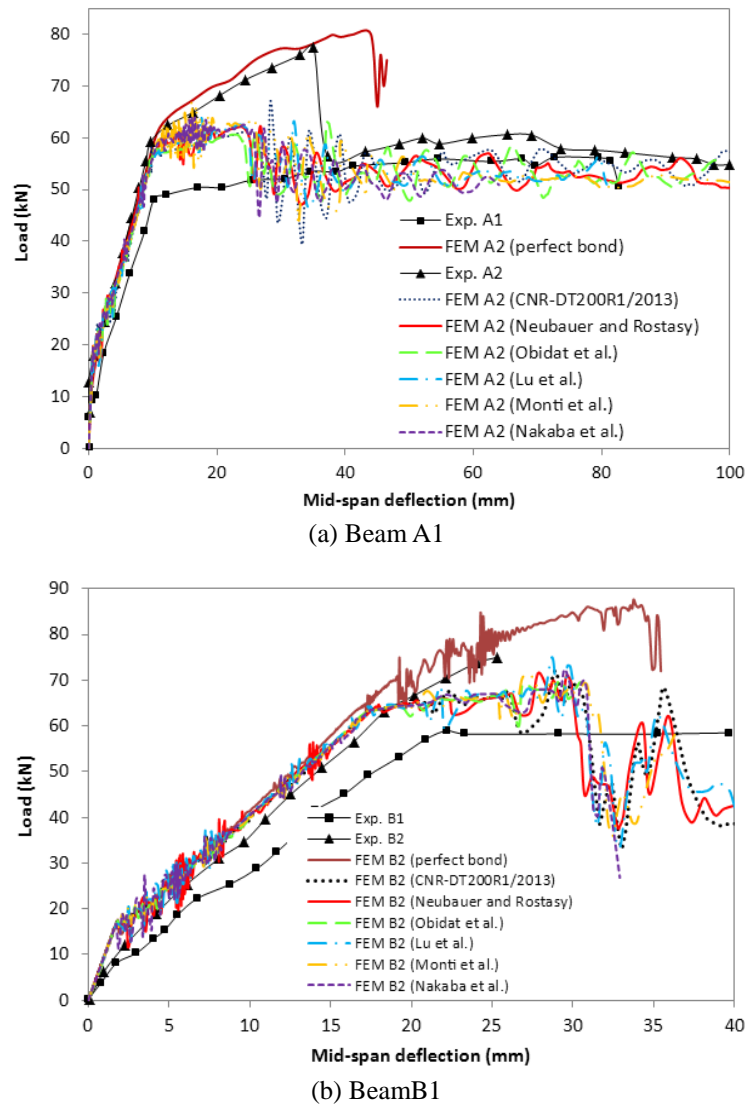


Fig. 12 Load-deflection behavior of strengthened beams A2 and B2

on bond-slip law of Monti *et al.* (2003) predicts the load capacity of the retrofitted beam A2 equal to 66.96 kN whereas the experimental value is 77.50 kN. For the retrofitted RC beam B2, the load capacity predicted by FE model is 70.62 kN while the experimental value is 75.01 kN. Note that the failure mode of the beam A2 is CFRP debonding (Qeshta *et al.* 2015) while the failure mode of the beam B2 is concrete crushing followed by CFPP debonding (Rahimi and Hutchinson 2001). It seems that the error of the present FE models in the prediction of the load capacity of the retrofitted beams with pure CFRP debonding failure modes is higher than those with other failure modes. There are various possible causes for the differences between the experimental and the FE results. The assumption of the perfect bond between the concrete and reinforcing steels may be one of these reasons. The improper approximation of the bond-slip law parameters (e.g., initial stiffness of bond-slip curve, fracture energy, initiation damage criterion, and the type of failure criterion under mixed-mode conditions) may be the other sources of discrepancy.

A comparison between the numerical and experimental crack patterns of the retrofitted RC beam A2 at the failure load is given in Fig. 13. Detail of the CFRP sheet detachment from the beam A2 is shown in Fig. 14.

It is seen from these figures that the present FE model is very good in the simulation of the detachment of the CFRP from beam as well as the prediction of the crack patterns. Fig. 15 shows the distributions of the tensile and compressive cracks in the RC beam B2 at the failure load. It can be observed that the failure mode of this retrofitted RC beam (concrete crushing followed by CFRP debonding) is captured well using the present FE model.

Fig. 16 shows the mid-span strains of reinforcing steels in specimens A2 and B2. Distributions of the axial stress in the CFRP sheets and reinforcing steels at different load levels are also given in Figs. 17 and 18. It can be seen that the stress in the reinforcing steels and CFRP sheets does not increase uniformly in the constant moment region due to appearing the tensile cracks in the concrete. Distributions of the interfacial slips in samples A2 and B2 are shown in Fig. 19 at different deflection levels. It can be observed that the

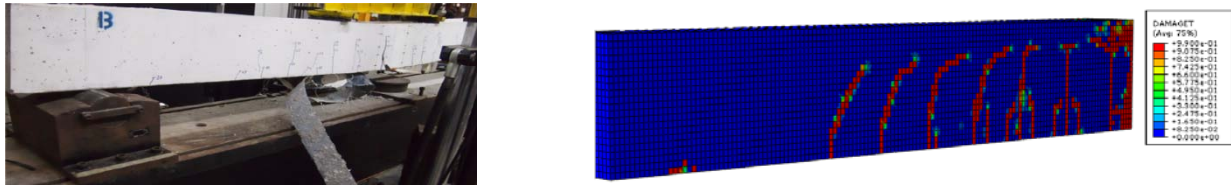


Fig. 13 Numerical and experimental comparison of the cracking pattern in beam A2 at the failure load

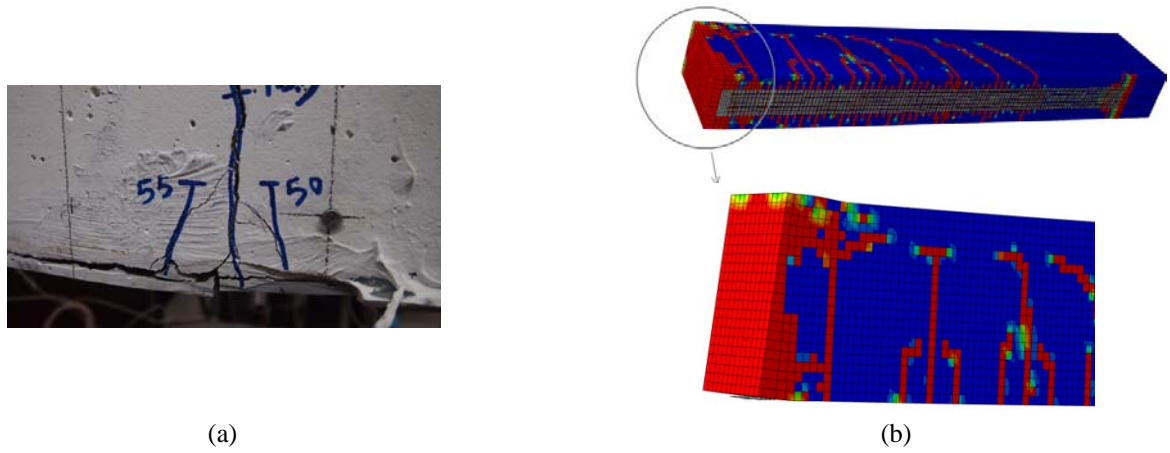


Fig. 14 Details of the CFRP detachment at mid-span after rupture in specimen A2: (a) experimental model; (b) FE model

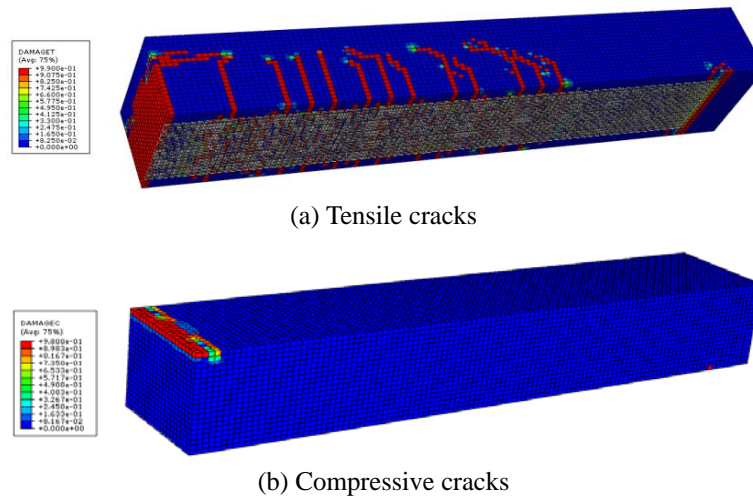


Fig. 15 Distributions of cracks in the RC beam B2 at the failure load

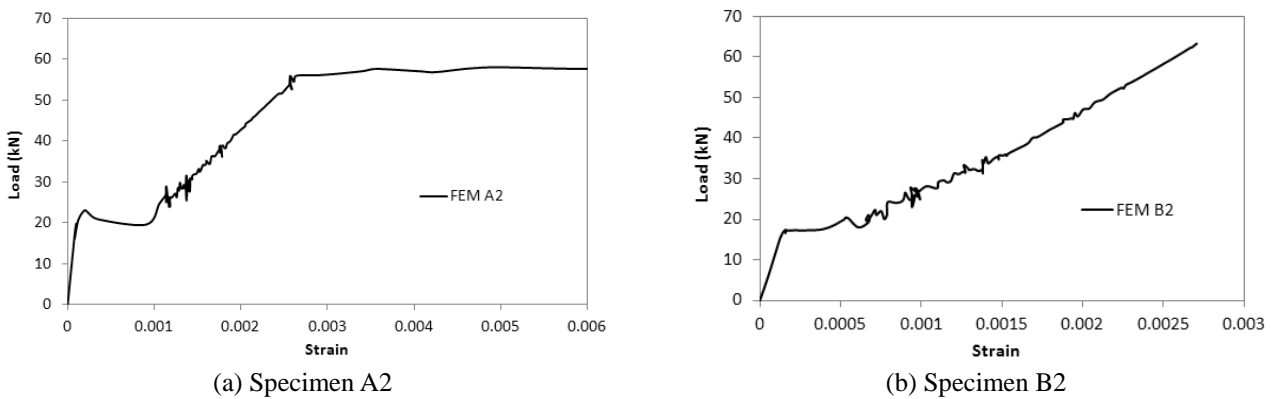
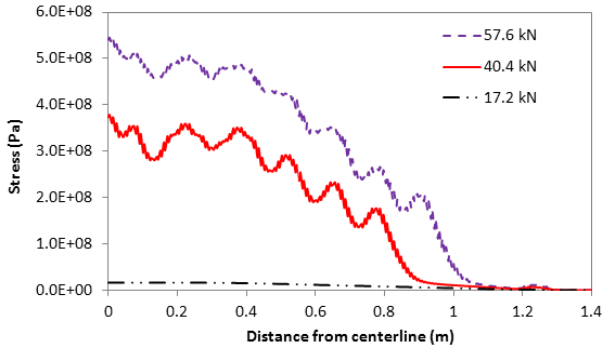
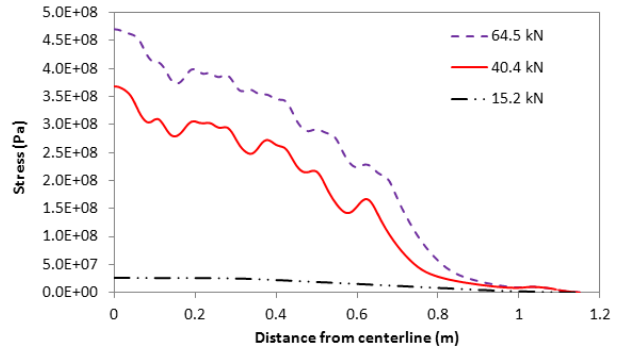


Fig. 16 Variations of the mid-span strains of reinforcing steels against the applied load

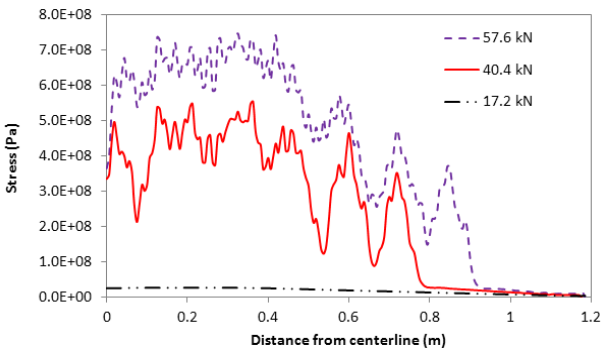


(a) Sample A2

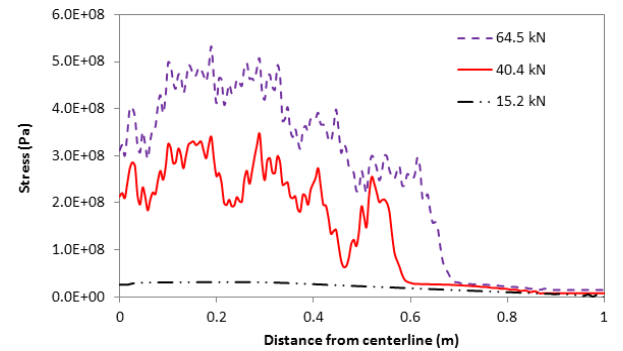


(b) Sample B2

Fig. 17 Distributions of stress in the reinforcing steels at different loading levels

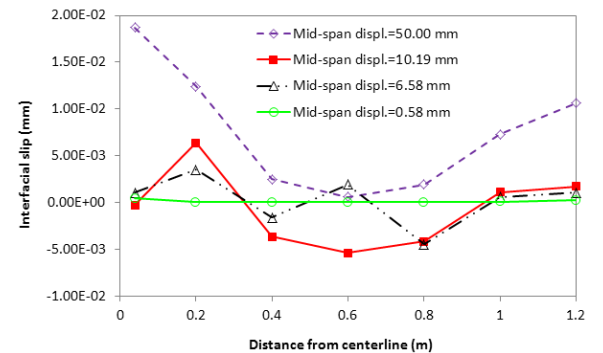


(a) Sample A2

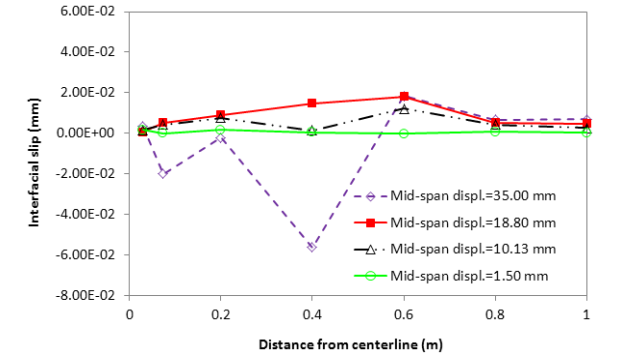


(b) Sample B2

Fig. 18 Distributions of stress in the CFRP sheets at different loading levels

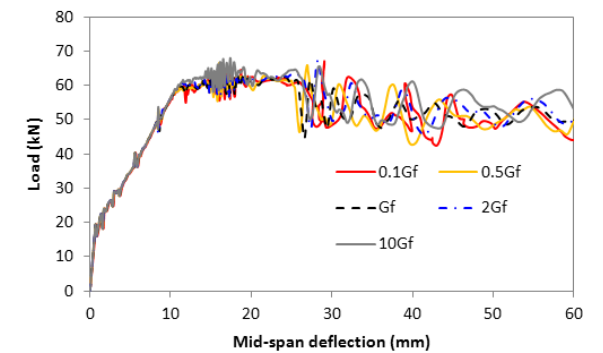


(a) Sample A2

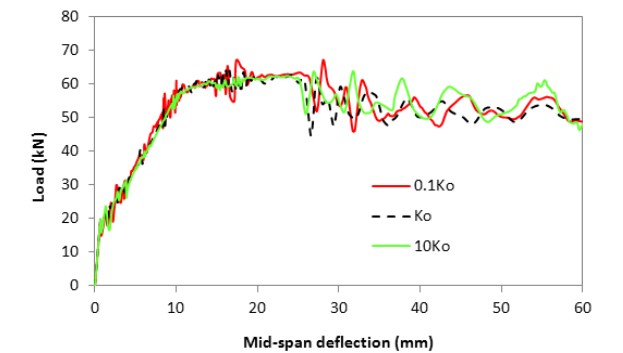


(b) Sample B2

Fig. 19 Interfacial slip at different deflection levels



(a) Interfacial fracture energy



(b) Initial stiffness of the interface

Fig. 20 Sensitivity to the bond-slip parameters

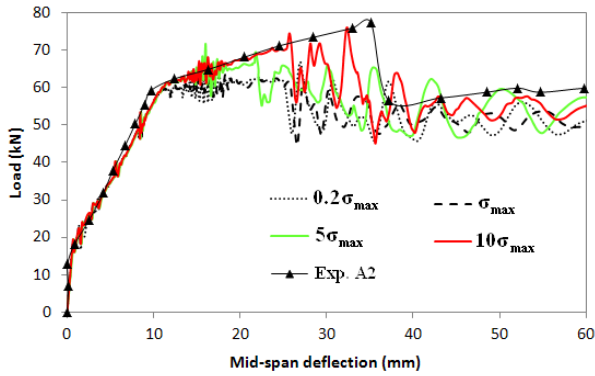


Fig. 21 Sensitivity to the maximum interfacial stress values

significant slips occur at the interface between CFRP and concrete even times that the retrofitted RC beams are under the action of service loads.

5.3 Sensitivity study (bond-slip parameters)

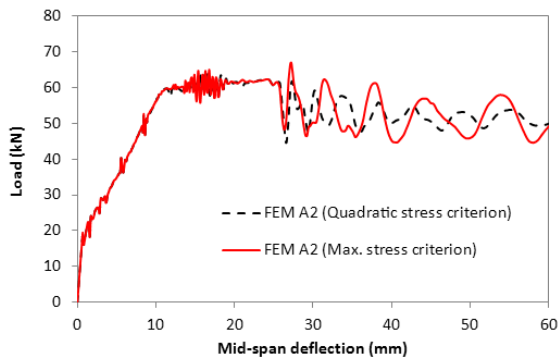
In this section, the sensitivity of the FE results is investigated with respect to the bond-slip parameters (i.e., initial stiffness of bond-slip curve, fracture energy, cohesive property coefficient, maximum interfacial stress, initiation damage criterion, and the type of failure criterion under mixed-mode conditions). The numerical results obtained for the retrofitted beam A2 with Nakaba's bond-slip model (Nakaba *et al.* 2001) is used here for the illustration

purposes.

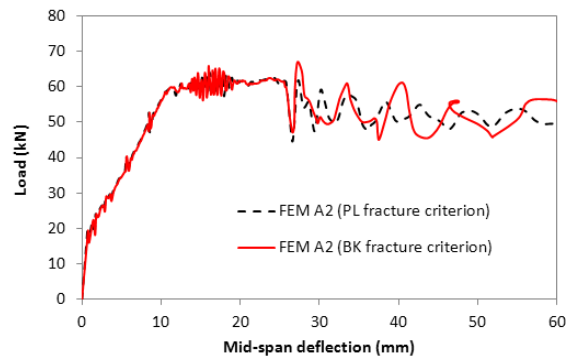
The sensitivity of the numerical results against the CFRP/concrete interfacial fracture energy is investigated in Fig. 20(a) in the framework of load-deflection response. In this figure, the interfacial fracture energy was changed from $0.1G_f$ to $10G_f$. The initial stiffness of the interface was also changed from $0.1K_0$ to $10K_0$. The numerical results are shown in Fig. 20(b). It is seen that the numerical results are almost insensitive to changes of G_f and K_0 .

The effect of the maximum interfacial stress values on the global response of the retrofitted beam A2 is investigated in Fig. 21. In this figure, the value of the maximum interfacial stress is changed from $0.2\sigma_{max}$ to $10\sigma_{max}$. Numerical results shown in Fig. 21 indicate that the peak load of the curve is significantly affected by the maximum interfacial stress value. With increasing the maximum interfacial stress, the discrepancy between the present FE results and experimental data reduces. This shows that the Nakaba's bond-slip law as well as the other similar interfacial models evaluated in the previous sections underestimates the ultimate strength of CFRP/concrete interface. It seems that the traditional single or double lap shear pullout tests employed for the evaluation of the bond action between CFRP and concrete are not satisfactory.

The sensitivity of the results with respect to the type of the initiation damage criterion is also investigated. The load-deflection curves of the beam A2 with Maximum stress and Quadratic stress criteria are depicted in Fig. 22(a).

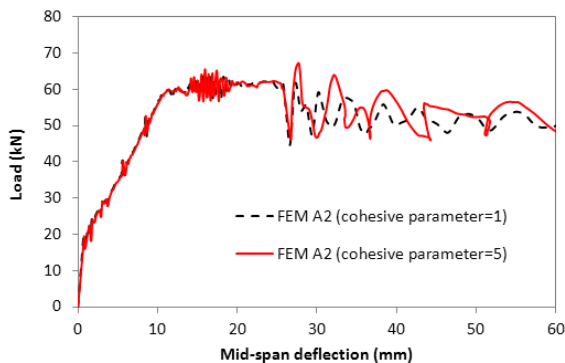


(a) Type of the initiation damage criterion

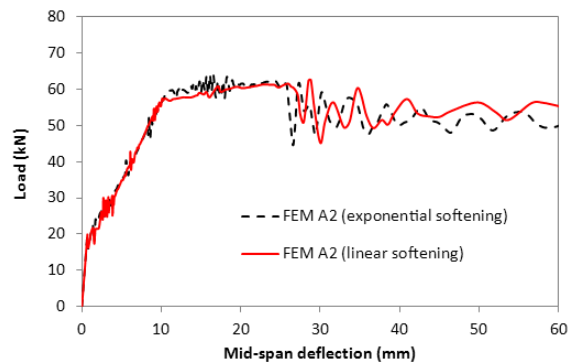


(b) Type of mixed-mode failure criterion

Fig. 22 Sensitivity to the bond-slip parameters



(a) Cohesive property coefficient



(b) Type of softening curve

Fig. 23 Sensitivity to the bond-slip parameters

The sensitivity of the FE results against the type of failure criterion under mixed-mode conditions is also investigated in Fig. 22(b). In this figure, the load-deflection curves obtained based on the BK and PL fracture criteria are compared with each other. It can be observed from Fig. 22 that the peak load and generally the global response of the retrofitted RC beams are not affected by the type of the initiation damage criterion or the type of mixed-mode failure criterion.

The sensitivity of the numerical results against the type of the softening curve of the bond-slip model is investigated in Fig. 23(a). In this figure, the load-deflection of the retrofitted RC beam A2 is depicted with considering both linear and exponential softening curves for the bond-slip model. The sensitivity of the FE results with respect to the value of the cohesive property coefficient η is also studied in Fig. 23(b). It can be observed that the numerical results are insensitive to these interface parameters.

6. Conclusions

The effectiveness of different FRP/concrete bond–slip laws for the prediction of the structural behavior of externally strengthened RC beams was evaluated in this study. To this aim, an FE model was developed for the nonlinear analysis of the retrofitted RC beams. The main practical conclusions of the present paper may be summarized as follows:

- The use of high values for the viscosity parameter leads to the diffuse pattern of cracking which limits the real crack propagation procedure.
- The ultimate load capacity of the un-strengthened RC beams is almost insensitive to the changes of the concrete tensile strength.
- A perfect bond model leads to the overestimation of the ultimate load capacity of the retrofitted RC beams. It also fails to capture the softening behavior of the retrofitted beams.
- No significant differences were observed in the predicted structural responses of the retrofitted RC beams when different bond-slip models were used.
- No significant changes were observed in the global response of the RC beams strengthened with CFRP when different damage criteria were used for the bond-slip law.
- The type of the failure criterion selected for describing the dependency of the interfacial fracture energy to the opening and sliding failure modes does not affect the global response of the retrofitted beams.
- Peak loads of the strengthened RC beams are not affected significantly by changing the values of FRP/concrete interfacial fracture energy.
- The global response of the RC beams strengthened with FRP is not sensitive to the changes of neither the initial stiffness of the bond-slip curve nor the cohesive coefficient of the interface.
- The available bond-slip models underestimate the strength of FRP/concrete interface. For accurate simulation of the FRP-debonding failures, the modification of the present bond-slip laws is essential. The response of the retrofitted beams is very sensitive to the changes of the maximum interfacial stresses. The appropriate values of this parameter are needed for the accurate prediction of the FRP-debonding failures.
- The structural response of the retrofitted beams is insensitive to the type of the softening curve of the bond-slip model.

References

- Hibbitt, Karlsson and Sorensen, Inc. (2000) ABAQUS theory manual, user manual and example manual; Version 6.7, Providence, RI, USA.
- Abdel Baky, H., Ebead, U.A. and Neale, K.W. (2012), “Nonlinear micromechanics-based bond–slip model for FRP/concrete interfaces”, *Eng. Struct.*, **39**, 11-23.
- ACI 440.2R-02 (2002), Guide for the design and construction of externally bonded FRP systems for strengthening concrete structures, American Concrete Institute; Farmington Hills, MI, USA.
- Arduini, M., Di Tommaso, A. and Nanni, A. (1997), “Brittle failure in FRP plate and sheet bonded beams”, *ACI Struct. J.*, **94**(4), 363-370.
- Bencardino, F. and Condello, A. (2015), “SRG/SRP–concrete bond–slip laws for externally strengthened RC beams”, *Compos. Struct.*, **132**, 804-815.
- Biolzi, L., Ghittoni, C., Fedele, R. and Rosati, G. (2013), “Experimental and theoretical issues in FRP-concrete bonding”, *Constr. Build. Mater.*, **41**, 182-190.
- Bocciarelli, M. and Pisani, M.A. (2015), “Modified force method for the nonlinear analysis of FRP reinforced concrete beams”, *Compos. Struct.*, **131**, 645-653.
- Chen, W.F. (1982), *Plasticity in Reinforced Concrete*, XV, McGraw-Hill, New York, NY, USA.
- Chen, G.M., Chen, J.F. and Teng, J.G. (2012), “On the finite element modelling of RC beams shear-strengthened with FRP”, *Constr. Build. Mater.*, **32**, 13-26.
- Chen, G.M., Chen, J.F. and Teng, J.G. (2012), “Behaviour of FRP-to-concrete interfaces between two adjacent cracks: A numerical investigation on the effect of bondline damage”, *Constr. Build. Mater.*, **28**(1), 584-591.
- CNR-DT 200 R1/2013 (2013), Guide for the design and construction of externally bonded FRP systems for strengthening existing structures – materials, RC and PC structures, masonry structures; Italian National Research Council, Rome, Italy.
- Coronado, C.A. and Lopez, M.M. (2006), “Sensitivity analysis of reinforced concrete beams strengthened with FRP laminates”, *Cem. Concrete Compos.*, **28**(1), 102-114.
- Colombi, P., Fava, G. and Poggi, C. (2014), “End debonding of CFRP wraps and strips for the strengthening of concrete structures”, *Compos. Struct.*, **111**, 510-521.
- Hognestad, E. (1951), “A study of combined bending and axial load in reinforced concrete members”, Bulletin series No. 399, Engineering Experiment Station, **49**(22).
- Kupfer, H., Hilsdorf, H.K. and Rusch, H. (1969), “Behavior of concrete under biaxial stresses”, *ACI Mater. J.*, **66**(8), 656-666.
- Lee, J. and Fenves, G.L. (1998), “Plastic-damage model for cyclic loading of concrete structures”, *J. Eng. Mech.*, **124**(8), 892-900.
- Lezgy-Nazargah, M. (2017), “Assessment of refined high-order global-local theory for progressive failure analysis of laminated composite beams”, *Acta Mech.*, **228**(5) 1923-1940

- Lu, X.Z., Teng, J.G., Yea, L.P. and Jiang, J.J. (2005), "Bond-slip models for FRP sheets/plates bonded to concrete", *Eng. Struct.*, **27**(6), 920-937.
- Lublinter, J., Oliver, J., Oller, S. and Oñate, E. (1988), "A plastic-damage model for concrete", *Int. J. Solids Struct.*, **25**(3), 299-326.
- Mazzotti, C., Savoia, M. and Ferracuti, B. (2008), "An experimental study on delamination of FRP plates bonded to concrete", *Constr. Build. Mater.*, **22**(7), 1409-1421.
- Monti, M., Renzelli, M. and Luciani, P. (2003), "FRP adhesion in uncracked and cracked concrete zones", *Proceedings of the 6th International Symposium on Fiber Reinforced Polymer Reinforcement for Concrete Structures*, (KH Tan Editor), National University of Singapore, Singapore, July, pp. 183-192.
- Nakaba, K., Toshiyuki, K., Tomoki, F. and Hiroyuki, Y. (2001), "Bond behavior between fiber-reinforced polymer laminates and concrete", *ACI Struct. J.*, **98**(3), 359-367.
- Neubauer, U. and Rostasy, F.S. (1999), "Bond failure of concrete fiber reinforced polymer plates at inclined cracks-experiments and fracture mechanics model", *Proceedings of the 4th International Symposium on Fiber Reinforced Polymer Reinforcement for Reinforced Concrete Structures, SP-188*, Baltimore, MD, USA, November, pp. 369-382.
- Obaidat, Y.T., Heyden, S. and Dahlblom, O. (2010), "The effect of CFRP and CFRP/concrete interface models when modelling retrofitted RC beams with FEM", *Compos. Struct.*, **92**(6), 1391-1398.
- Obaidat, Y.T., Heyden, S. and Dahlblom, O. (2013), "Evaluation of parameters of bond action between FRP and concrete", *J. Compos. Constr.*, **17**(5), 626-635.
- Panjehpour, M., Abang Ali, A.A. and Nora Aznieta, F. (2014), "Energy absorption of reinforced concrete deep beams strengthened with CFRP sheet", *Steel Compos. Struct., Int. J.*, **16**(5), 481-489.
- Qeshta, I.M.I., Shafiqh, P. and Jumaat, M.Z. (2015), "Flexural behaviour of RC beams strengthened with wire mesh-epoxy composite", *Constr. Build. Mater.*, **79**, 104-114.
- Rahimi, H. and Hutchinson, A. (2001), "Concrete beams strengthened with externally bonded FRP plates", *J. Compos. Constr.*, **5**(1), 44-56.
- Uriayer, F.A. and Alam, M. (2015), "Steel-CFRP composite and their shear response as vertical stirrup in beams", *Steel Compos. Struct., Int. J.*, **18**(5), 1145-1160.
- Wang, Y.C. and Chen, C.H. (2003), "Analytical study on reinforced concrete beams strengthened for flexure and shear with composite plates", *Compos. Struct.*, **59**(1), 137-148.
- Wang, Q. and Shao, Y. (2014), "Compressive performances of concrete filled Square CFRP-Steel Tubes (S-CFRP-CFST)", *Steel Compos. Struct., Int. J.*, **16**(5), 455-480.
- Wong, R.S.Y. and Vecchio, F.J. (2003), "Towards modeling of reinforced concrete members with externally bonded fiber-reinforced polymer composites", *ACI Struct. J.*, **100**(1), 47-55.
- Zhou, C., Lu, X., Li, H. and Tian, T. (2014), "Restoring force model for circular RC columns strengthened by pre-stressed CFRP strips", *Steel Compos. Struct., Int. J.*, **17**(4), 371-386.
- Ziraba, Y.N. and Baluch, M.H. (1995), "Computational model for reinforced concrete beams strengthened by epoxy bonded steel plates", *Finite Elem. Anal. Des.*, **20**(4), 253-271.